Bioresource Technology 292 (2019) 121937

Contents lists available at ScienceDirect

Bioresource Technology

journal homepage: www.elsevier.com/locate/biortech

Enhancement of β-carotene production by regulating the autophagy-carotenoid biosynthesis seesaw in *Chlamydomonas reinhardtii*

Quynh-Giao Tran[a,b], Kichul Cho[c], Urim Kim[a,b], Jin-Ho Yun[a], Dae-hyun Cho[a], Jina Heo[a,b], Su-Bin Park[a,b], Ji Won Kim[a,b], Yong Jae Lee[a], Rishiram Ramanan[d], Hee-Sik Kim[a,b,*]

[a] Cell Factory Research Center, Korea Research Institute of Bioscience and Biotechnology (KRIBB), Daejeon 34141, Republic of Korea
[b] Department of Environmental Biotechnology, KRIBB School of Biotechnology, University of Science & Technology (UST), Daejeon 34113, Republic of Korea
[c] Environmental Safety Group, Korea Institute of Science and Technology (KIST) Europe, Campus E 7.1, 66123 Saarbrücken, Germany
[d] Department of Environmental Science, Central University of Kerala, Kasaragod, Kerala, India

GRAPHICAL ABSTRACT

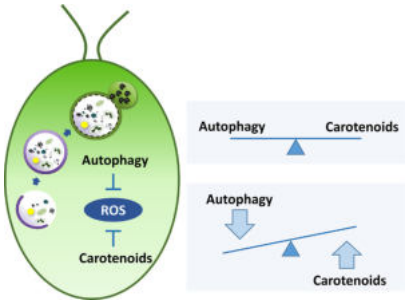

ARTICLE INFO

Keywords:
Artificial microRNA
Autophagy
Biodiesel properties
Carotenoids
Chlamydomonas reinhardtii

ABSTRACT

This work aimed to demonstrate a new strategy for enhancing the production of carotenoids through the regulation of seesaw cross-talk between autophagy and carotenoid biosynthesis pathways in *Chlamydomonas reinhardtii*. Autophagy-related *ATG1* and *ATG8* genes were first silenced using artificial microRNA, which in turn reduced the mRNA expression of *ATG1* and *ATG8* by 84.4% and 74.3%, respectively. While ATG1 kinase controls early step in autophagy induction and ATG8 is an essential factor for the downstream formation of autophagosome membranes, the decreased expression of these genes led to a 2.34-fold increase in the amount of β-carotene content (i.e., 23.75 mg/g DCW). Furthermore, all mutants seemed to exhibit greater biodiesel properties than that of wild-type due to increased accumulation of saturated and monounsaturated fatty acids. These results support the role of autophagy in regulating the production of valuable metabolites, which could contribute to uplifting the economic outlook of nascent algal biorefinery.

1. Introduction

Carotenoids are natural tetraterpenoid pigments distributed widely in plants, algae, fungi, and bacteria (Lohr, 2009). In photosynthetic organisms, carotenoids play essential roles in light capture and photoprotection. Indeed, a variety of carotenoids including carotene and xanthophyll are known to improve light harvesting efficiency of the photosystem II in plants and algae by absorbing and transferring light energy from different wavelengths to chlorophylls, while they also dissipate excess light energy through vibration when cells are exposed

* Corresponding author at: Cell Factory Research Center, Korea Research Institute of Bioscience and Biotechnology (KRIBB), Daejeon 34141, Korea.
E-mail address: hkim@kribb.re.kr (H.-S. Kim).

https://doi.org/10.1016/j.biortech.2019.121937
Received 12 June 2019; Received in revised form 29 July 2019; Accepted 30 July 2019
Available online 01 August 2019
0960-8524/

to high irradiance (Gong and Bassi, 2016; Takaya et al., 2018). In addition, carotenoids act as strong antioxidants which can deactivate reactive oxygen species (ROS) generated under stress conditions, especially peroxyl radicals, by reacting with them to reach a more stable energy state (Fiedor and Burda, 2014; Nimse and Pal, 2015). Therefore, the onset of ROS-associated chronic diseases ranging from cardiovascular disease to cancers were demonstrated to be mitigated by carotenoid pigments (Fiedor and Burda, 2014).

A recent survey underscored that the global market value of carotenoids would reach ca. 1.53 billion USD by 2021 as global demand for health supplements increase by leaps and bounds (Sathasivam and Ki, 2018). While the commercial production of carotenoids is currently centered around chemical synthesis or extraction from plants, microbe-based production of carotenoids could be a cost-effective alternative due to high growth capacity of microbes and the possibility of incorporating agro-industrial wastes into the production of high-value carotenoids (Mata-Gómez et al., 2014). In particular, the production of carotenoid pigments such as lutein, astaxanthin, zeaxanthin, fucoxanthin and β-carotene from photosynthetic microalgae has been demonstrated in previous studies, and the results indicated a great potential of microalgae as a feedstock for carotenoids production (Borowitzka, 2013).

In recent years, great efforts have been made to increase the productivity of algal carotenoids. For instance, a two-phase cultivation strategy in which a short period of nitrogen starvation followed by high illumination during phase-two resulted in superior production of both carotenoids and nutritional protein in *Dunaliella salina* (Sui et al., 2019). Additionally, strategies of combining abiotic stress conditions and phytohormones have been found to promote carotenoids production in *Haematococcus pluvialis*, *Nostoc muscorum* and *Chlorella vulgaris* (Zhao et al., 2019). These approaches, however, would necessitate costly management of operational conditions (Sun et al., 2018b); therefore, the prime focus of industrial biotechnology aims at developing suitable microorganisms with a variety of genetic engineering strategies (Sun et al., 2018b).

Overexpressing genes involved in the biosynthesis of carotenoid precursors or enzymes is acknowledged as one of the most common approaches to enhance the production of carotenoids by regulating the rate-limiting steps in carotenoid synthesis pathway (Gimpel et al., 2015; Minhas et al., 2016). Although moderate successes have been reported from these strategies, ectopic expression of transgenes is sometimes subjected to reversibly suppressed, either by post-transcriptional regulation or chromatin-mediated gene silencing, hindering stable genetic modification of microalgae (Molnar et al., 2009). Nonetheless, RNA silencing can provide a powerful alternative to facilitate effective genetic modification of microalgae. In particular, it has been shown that artificial microRNAs (amiRNA), which are short non-coding RNA molecules of 21–22 nucleotides, can overcome the problems associated with self-silencing and specifically suppress single or multiple genes of interest in *C. reinhardtii* (Molnar et al., 2009).

Recently, the role of autophagy, a conversed self-recycling mechanism throughout eukaryotes, in microalgae has attracted much attention because of its role in cleaning up senescent or oxidized cellular components that would otherwise lead to an oxidative chain reaction and trigger cell death (Giordano et al., 2013; Pérez-Pérez et al., 2017). In particular, previous studies have suggested the interplay between autophagy and carotenoids in microalgae. Zhang and his colleagues, for example, reported that chemical inhibition of autophagy led to the accumulation of astaxanthin in *Chlorella zofingiensis* in order to reduce the effect of elevated ROS levels under nitrogen starvation (Zhang et al., 2018). Corroborating with their results, blocking carotenoid synthesis was demonstrated to enhance autophagic activity in *C. reinhardtii* as a result of increased ROS accumulation due to the lack of available ROS scavengers (Pérez-Pérez et al., 2012). All above evidences support the hypothesis that autophagy and carotenoid pathways could act in a manner of seesaw cross-talk model to prevent cellular oxidative damage. In other words, a reduction in one side of the metabolic seesaw could enhance the activity of the other side to compensate a loss in overall protective capacity. To further explore this hypothesis, amiRNAs were used to generate mutants with lower autophagy activity in *C. reinhardtii*. Thereafter, the impact of a reduction in autophagy activity on carotenoids, lipid content and fatty acids synthesis under nitrogen starvation was examined. Combined together, the results allow us to propose a new strategy to enhance the production of desirable metabolites by effectively regulating two paired metabolic pathways in microalgae.

2. Materials and methods

2.1. Growth conditions

Chlamydomonas reinhardtii CC-124 wild-type [137c] were obtained from the *Chlamydomonas* Resource Center (University of Minnesota, USA). All strains were grown on Tris-acetate phosphate (TAP) medium under continuous illumination of 100 ± 10 μmol/m^2/s at 25 °C and shaken at 90 rpm. For solid medium, bacto agar was added to a final concentration of 15 g/L. In the nitrogen starvation experiments, cells in exponential phase (approximately 1×10^6 cells/ml) were harvested, washed twice in nitrogen-free TAP medium before resuspension to the same cell density. For screening of transformants, paromomycin (Sigma-Aldrich, USA) was used at a concentration of 25 μg/ml.

2.2. Transformation and selection of knockdown mutants

The amiRNA-based gene silencing system (pChlamiRNA3int) was used to suppress the expression of *ATG1* or *ATG8* gene in *C. reinhardtii* (Molnar et al., 2009). The miRNAs were designed using the Web MicroRNA Designer 2 (WMD2) web-based tool (Molnar et al., 2009; Ossowski et al., 2008) (Table 1). The oligos encoding these miRNAs were synthesized and cloned into pChlamiRNA3int vector, which also carries a paromomycin-resistance cassette, following the protocol described previously (Molnar et al., 2009). The resultant vectors were transformed in *C. reinhardtii* using electroporation and putative transformants were selected by their resistance to paromomycin. qPCR analysis was carried out to access the suppression ability of these miRNA on the target genes in the selected transformants.

2.3. Expression analysis by qPCR

Cells were harvested by centrifugation and snap frozen with liquid nitrogen before storage at −80 °C. Total RNA was extracted with TRIzol® Reagent (Ambion, USA) and purified with QIAGEN RNeasy Mini Kit (QIAGEN, Germany) in accordance with the manufacturer's protocol. RNA purity and quantity were checked with the NanoPhotometer® P360 device (Implen, Germany) after removal of genomic DNA contamination using RQ1 RNase-Free DNase kit (Promega, USA). First-strand cDNA was synthesized using GoScript™ Reverse Transcription System (Promega, USA) with oligo (dT) primer from 500 ng of total RNA per sample. The resulting cDNA was used as template for real-time qPCR using iQ™ SYBR® Green Supermix (Biorad, USA) with the primers listed in Table 1.

2.4. Determination of growth rate and biomass productivity

The optical density at 680 nm (OD_{680}) was measured on a spectrophotometer (Tecan, Switzerland) for monitoring cell growth. Cell numbers were counted using a C-Chip hemocytometer (NanoEnTek, USA). Dry cell weight was determined daily by passing 5 ml of the cell culture on a pre-dried and pre-weighted GF/C filter paper (Whatman, UK). After rinsing twice with distilled water, the filter papers containing algal biomass were dried at 105 °C for overnight and weighed again. The dry weight was calculated by subtracting the weight of empty filter

Table 1
List of oligonucleotides used in this study.

Oligo	Sequence (5′ to 3′)	Mutant name
Artificial microRNAs designed to target different position of the ATG1 and ATG8 mRNAs		
AMI-ATG1-1F	ctagtTGGGAGTACGCTTTATGTGGAtctcgctgatcggcaccatgggggtggtggtgatcagcgctaTCCATGTAAAGCGTACTCCCAg	K1, K2
AMI-ATG1-1R	ctagcTGGGAGTACGCTTTACATGGAtagcgctgatcaccaccacccccatggtgccgatcagcgagaTCCACATAAAGCGTACTCCCAa	
AMI-ATG1-2F	ctagtCTGACGGATTGAACAACAAGAtctcgctgatcggcaccatgggggtggtggtgatcagcgctaTCTTCTTGTTCAATCCGTCAGg	K3, K4
AMI-ATG1-2R	ctagcCTGACGGATTGAACAAGAAGAtagcgctgatcaccaccacccccatggtgccgatcagcgagaTCTTGTTGTTCAATCCGTCAGa	
AMI-ATG8-1F	ctagtAGGCAATTTGTGTACGACATAtctcgctgatcggcaccatgggggtggtggtgatcagcgctaTATGACGTACACAAATTGCCTg	A1, A2
AMI-ATG8-1R	ctagcAGGCAATTTGTGTACGTCATAtagcgctgatcaccaccacccccatggtgccgatcagcgagaTATGTCGTACACAAATTGCCTa	
AMI-ATG8-2F	ctagtCAGGCCGAATTCCAGTGATTAtctcgctgatcggcaccatgggggtggtggtgatcagcgctaTAATGACTGGAATTCGGCCTGg	A3, A4
AMI-ATG8-2R	ctagcCAGGCCGAATTCCAGTCATTAtagcgctgatcaccaccacccccatggtgccgatcagcgagaTAATCACTGGAATTCGGCCTGa	
Primers for confirmation of amiRNA sequences		
ami_F	GGTGTTGGGTCGGTGTTTTT	
ami_R	CGGTGTAACTAAGCCAGCCC	
Primers for detection of paromomycin-resistance gene in microalgal transformants		
*APHVIII*_ F	AAGCTTCCATGGGATGACG	
*APHVIII*_ R	TCAGGCAGACGGGCAGGTG	
Primers for qPCR		
*ATG1*_18F	TCAACTGGATGAAAAATGGC	
*ATG1*_285R	CTGGTTCCTTAAAGAGGTCCAG	
*ATG8*_104F	CAGCATCTCCACAATGGTTGGC	
*ATG8*_239R	CTCTGCCTTCTCGACAATGACTGG	
*CBLP*_814F	GACGACCTGCGCCCCGAGTT	
*CBLP*_979R	AGGCGCGGCTGGGCATTTAC	

paper from the weight of filter paper with algal biomass.

The specific growth rate (μ) was calculated by Eq. (i):

$$\mu = ln\left(\frac{X_2}{X_1}\right) \times \frac{1}{t_2 - t_1} \quad \text{(i)}$$

where X_1 and X_2 were the cell densities of the cultivation at time t_1 and t_2, respectively.

The biomass productivity was calculated by Eq. (ii):

$$P = \frac{(X - X_0)}{(t - t_0)} \quad \text{(ii)}$$

where X and X_0 were the cell densities at the end (time t) and the beginning (time t_0) of the cultivation, respectively.

2.5. Total lipid extraction and fatty acid analysis

Total lipid was extracted from lyophilized cells as described by Blight and Dyer with some modifications (Bligh and Dyer, 1959). In brief, 10 mg of sample was mixed with 15 ml of chloroform–methanol mixture (1:2, v/v) in a glass vial. The mixtures were subjected to sonication for 5 min using Ultrasonic Cleaner (WiseClean, Korea). To each, 5 ml of chloroform was added, and the mixtures were vigorously shaken for 30 min using MMV-1000 W shaker (Eyela, Japan). Afterwards, 10 ml of distilled water was added to allow phase separation. The lower lipid-containing phase was obtained, filtered through 0.22 μm PTFE filters (Whatman, UK) and evaporated using a rotary evaporator (Buchi, Switzerland). The remaining lipid residue was precisely weighed using a microbalance.

A fatty acid composition analysis was performed following the method described by (Lee et al., 2010). The extracted lipid was saponified with 1 ml of saturated sodium hydroxide–methanol solution at 75 °C for 10 min, followed by methanolysis with 2 ml of 5% hydrochloric acid (in methanol, v/v) at 75 °C for another 10 min. Fatty acid methyl esters (FAME) recovery was obtained by adding 1.5 ml of hexane–methyl *tert*-butyl ether mixture (1:1, v/v). The bottom phase was removed, and the top phase was washed with 3 ml of base wash solution (10.8 g of sodium hydroxide dissolved in 900 ml of distilled water). Two-thirds of the upper phase was filtered and transferred to GC vial and capped for analysis using gas chromatography (Shimadzu GC-2010, Japan).

Biodiesel properties including cetane number (CN), iodine value (IV) and oxidation stability were calculated following the equations described previously (Islam et al., 2013).

2.6. Pigment extraction and composition analysis

Total pigments were extracted from lyophilized cells following the protocols described by (Heo et al., 2018; Yun et al., 2019). In brief, 10 mg of sample was mixed with 1 ml of ethanol and homogenized by bead beating with 0.1 mm and 0.5 mm zirconia beads (1:3, v/v) for two cycles of 20 s with 1 min interval rest on ice. The extracts were centrifuged at 10,000 × *g* for 10 min and the supernatants were filtered through 0.22 μm PTFE filters (Whatman, UK) and transferred to HPLC vial for analysis using the Agilent 1260 Infinity Binary LC system (Agilent Tech., USA) equipped with a Waters Spherisorb® S5 ODS1 4.6 × 250 mm, 5 μm Cartridge Column (Massachusetts, USA). The analysis was conducted at 40 °C for 25 min with an injection volume of 20 μl. During the run, solvent mixture A comprising 14% 0.1 M Tris-HCl (pH 8.0), 84% acetonitrile, and 2% methanol (v/v/v) was used from 0 to 15 min. From 15 to 19 min, solvent mixture B comprising 68% methanol and 32% ethyl acetate (v/v) was used. A post-run from 19 to 25 min was performed with the initial solvent mixture. The flow rate was maintained constantly at 1.2 ml/min.

2.7. Protein preparation and western blot analysis

Protein extraction were performed with RIPA buffer supplemented with Protease Inhibitor Cocktail (Sigma-Aldrich, USA). Protein concentrations were determined using the Pierce BCA Protein Assay Kit (Thermo Fisher Scientific, USA) and same amounts of total protein (30 μg/sample) were separated on 15% SDS-PAGE gels. The gels were blotted onto PVDF membranes using a semi dry transfer system (Bio-Rad, USA). Western blot analysis was performed with anti-CrATG8 (Abcam, United Kingdom) and anti-α-tubulin (Sigma-Aldrich, United Kingdom) antibodies (1:2000). Anti-rabbit (Abcam, United Kingdom) and anti-mouse (Abcam, United Kingdom) secondary antibodies (1:10,000) were used to detect ATG8 and α-tubulin, respectively.

2.8. Quantification of ROS levels

Cellular ROS levels were measured following the protocol described in previous work (Tran et al., 2019). In brief, algal cells grown under optimal or starvation conditions were harvested and washed twice with PBS buffer (pH 7.0). The cells were then suspended in 1 ml PBS buffer containing 10 μM dichloro-dihydro-fluorescein diacetate (DCFH-DA) (Sigma-Aldrich, United Kingdom) and incubated for 30 min in the dark with gentle shaking. The DCFH-DA signals were measured at excitation 485 nm and emission 535 nm wavelength using a fluorescence microplate reader, and the ratio of DCFH-DA/OD_{680} are presented.

2.9. Statistical analysis

All experiments were conducted in triplicates. Data are presented as means ± (1.96 × standard error (SE)) for a 95% confidence interval unless otherwise indicated. The overlapping error bars indicate no significant difference (i.e., $p > 0.05$).

3. Results and discussion

3.1. Characterization of ATG1 and ATG8

Autophagy is a self-recycling mechanism in eukaryotic organism and mediated by ATG proteins. Most of the core factors of autophagy machinery are conserved in the green alga *C. reinhardtii* (Pérez-Pérez et al., 2017). Among these factors, ATG1 (Phytozome accession number: Cre09.g391245.t1.1) is one of the most upstream components that activates autophagy process through its kinase function. On the other hand, ATG8 (Phytozome accession number: Cre16.g689650.t1.2) plays an essential role in a later step of autophagosome formation (Pérez-Pérez et al., 2017). In *C. reinhardtii*, autophagy is induced in response to a wide range of stress conditions including nutrient starvation, oxidative stress, heavy metal exposure, high irradiation, and high salinity (Couso et al., 2018; Pérez-Pérez et al., 2017; Ramanan et al., 2018). Upon stress exposure, the ATG1 complex consisting of ATG1 and ATG13 receives integrating signals and transduces them to the downstream autophagy pathway (Pérez-Pérez et al., 2017; Wong et al., 2013). Subsequently, double membrane vesicles called autophagosomes are formed, which collect cellular wastes including oxidized components and old organelles for recycling. During this process, ATG8 is anchored to the autophagosome membrane through its phosphatidylethanolamine (PE) tail, which is crucial for the correct expansion and stability of the membrane (Nakatogawa et al., 2007). The autophagosome and its inner materials are then degraded inside the central vacuole as observed in plants, yeast, and microalgae, and provide nutrients to promote cell survival (Abeliovich and Klionsky, 2001; Couso et al., 2018; Liu and Bassham, 2012). Thus, these two essential autophagy components were selected to investigate the interplay between autophagy and carotenoids pathways in *C. reinhardtii*.

3.2. Generation of knockdown mutants using artificial miRNA

To generate knockdown mutants of *ATG1* or *ATG8* gene, two amiRNA sequences were designed to target different exons of each gene and transformed into *C. reinhardtii* wild-type cells (Table 1). Upon electroporation, transformants were initially selected on agar plates containing paromomycin at a concentration of 25 μg/ml, and colony PCR was used to confirm the integration of the amiRNA sequences and paromomycin-resistance gene in each colony with primers listed in Table 1. The successfully transformed colonies were repeatedly subcultured to liquid medium supplemented with paromomycin. After seven rounds of selection, four lines with *ATG1* knock down and four lines with *ATG8* knockdown were selected and subjected to qPCR analysis (Table 1 and Fig. 1). As shown in Fig. 1b, all tested transformants showed a reduction in gene expression level compared to that of wild-type grown under same condition. Among the amiRNA constructs, AMI-ATG1-1 and AMI-ATG8-1, which respectively target the fifth exon of the *ATG1* mRNA and the fourth exon of the *ATG8* mRNA, had the best performance for gene silencing (up to 84.4% and 74.3% knockdown efficiency, respectively) (Fig. 1). To reduce confusion in managing the mutant collection, the mutants were named after the protein functions where K stands for kinase and A stands for autophagosome; the *ATG1* knockdown lines of K1 and K2, and the *ATG8* knockdown lines of A1 and A2 were selected for further analyses.

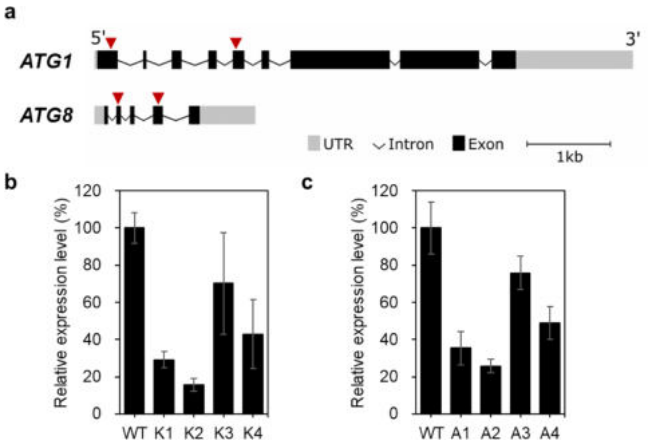

Fig. 1. Gene structures and expression analysis. (a) Schematic diagrams of *ATG1* and *ATG8* genes in *C. reinhardtii*. Arrowheads indicate target regions of the artificial miRNAs. (b–c) The relative expression levels of *ATG1* gene in *ATG1* knockdown mutants (b) or *ATG8* gene in *ATG8* knockdown mutants (c). The relative expression levels of target genes were checked over three generations and data are presented as means ± (1.96 × standard error (SE)) for a 95% confidence interval. The overlapping confidence intervals indicate no significant difference.

3.3. Growth rate comparison between wild-type and mutants

The effect of the respective knockdown of *ATG1* and *ATG8* genes on cell growth was examined in liquid culture. Under optimal growth condition, wild-type strain exhibited a steeper slope on the growth curve in comparison with mutants, indicating a higher growth rate during exponential phase (Fig. 2). However, there was no significant change in optical densities when each culture entered stationary phase (Fig. 2). The maximum specific growth rates were found to be 2.194, 1.861, 1.807, 1.908, and 1.815 for wild-type, mutant K1, K2, A1, and A2, respectively (Table 2). Among the mutants, A1 had the highest DCW of 1.73 ± 0.18 g/L, which was 93.5% of that of wild-type at the end of the cultivation (Table 2). Overall, the biomass productivities of mutants were slightly reduced by 7–20% compared to the wild-type, possibly due to low levels of nutrient recycling in those mutants.

3.4. Increase of β-carotene content in ATG8 knockdown mutants

Under nutrient starvation, microalgae stop growing and undergo a series of changes in metabolism to enhance survivability (Blaby et al., 2013). Notably, an increase in intracellular ROS has been observed under such conditions in diatoms and green algae (Liu et al., 2012; Yilancioglu et al., 2014). While accumulating evidence suggests that ROS functions as signaling messenger that mediates cell development and stress responses at low concentrations, it can indiscriminately damage lipids, proteins, and DNA once its concentration is increased to the level overwhelming the cellular antioxidant capacity (Ahmad et al., 2008; Menon et al., 2013; Schieber and Chandel, 2014; Shi et al., 2017). ROS-enriched cells thus produce non-enzymatic components including carotenoids along with antioxidant enzymes (e.g., superoxide dismutase (SOD), peroxidase (POD), catalase (CAT) and glutathione

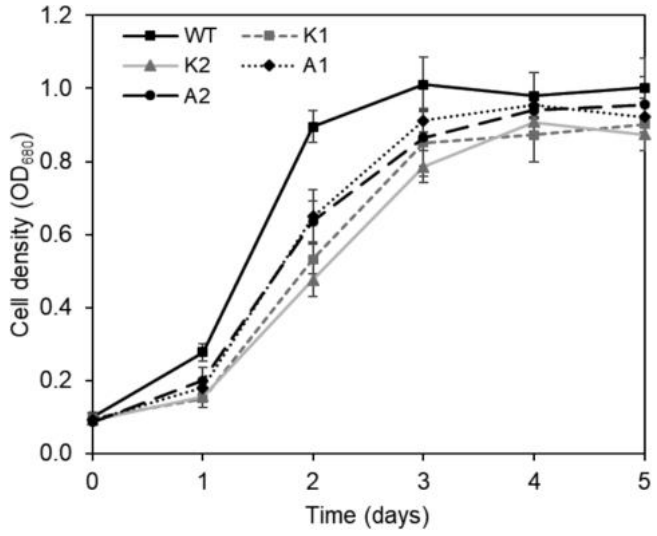

Fig. 2. Growth curve of wild-type and knockdown mutants. Mutants exhibited a delayed exponential phase growth, but similar optical cell densities compared to wild-type after reaching stationary phase. Error bars represent 95% confidence intervals of the means of three independent replicates. The overlapping confidence intervals indicate no significant difference.

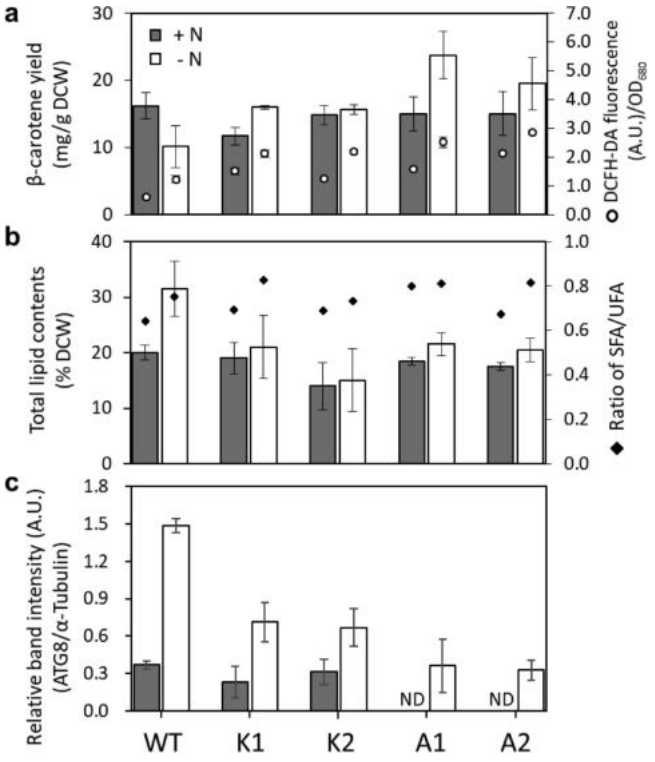

Fig. 3. The effect of autophagy knockdown on β-carotene and total lipid contents under nitrogen starvation. (a) β-carotene content. The open circles present cellular ROS levels, indicating by the relative DCFH-DA fluorescence normalized to OD_{680}. (b) Total lipid content. The black diamond symbols indicate the ratio of saturated fatty acids (SFA) to unsaturated fatty acids (UFA). (c) Relative autophagy activity based on ATG8 protein levels. Western blot images were quantified using ImageJ and the band intensity of ATG8 was normalized to the according α-Tubulin. The ATG8/α-Tubulin ratios were displayed. Error bars represent 95% confidence intervals of the means of three independent replicates. The overlapping confidence intervals indicate no significant difference.

reductase (GR)) to mitigate the damaging activity of ROS (Mallick and Mohn, 2000). Notably, autophagy is also induced to remove the oxidized components in order to terminate the chain reaction (Filomeni et al., 2015), suggesting a critical role of each of autophagy and antioxidant carotenoids in protecting cells from oxidative damages under stress conditions.

To evaluate the influence of *ATG* genes knockdown on carotenoids productivity in *C. reinhardtii*, wild-type and mutants at the same growth stage were subjected to nitrogen starvation for 6 days before carotenoids composition was analyzed. As shown in Fig. 3a, the β-carotene levels of K1, K2, A1, and A2 mutants under nitrogen starvation were 1.58-, 1.55-, 2.34-, and 1.93-fold higher than wild-type, respectively (Fig. 3a). This shift in carotenoids composition was notably different with what was observed in wild-type: the total amount of carotenoids in wild-type was reduced from 25.90 mg/g DCW under N-repletion to 14.51 mg/g DCW under N-starvation (Table 3), whereas total carotenoids contents were unchanged or slightly reduced in the mutants K1 (20.96–21.44 mg/g DCW) and K2 (23.29–20.11 mg/g DCW), and even increased in the mutants A1 (22.46–28.99 mg/g DCW) and A2 (23.66–25.65 mg/g DCW). Overall, β-carotene made the greatest contribution to the difference in total carotenoids content between wild-type and mutants. In addition, while ROS contents remained relatively low in WT, the amount of ROS in each of knockdown mutants was significantly higher, suggesting the role of autophagy in controlling cellular ROS levels in microalgae (Fig. 3a).

While previous studies showed that nitrogen starvation triggers lipid accumulation in *C. reinhardtii*, the influence of autophagy knockdown on lipid contents was further examined (López García de Lomana et al., 2015; Valledor et al., 2014). Corroborating with the existing literature, nitrogen starvation resulted in a 1.58-fold increase in total lipid content of wild-type cells (Fig. 3b). On the contrary, lipid production was not significantly increased in knockdown mutants after shifting to nitrogen starvation (Fig. 3b). It should be noted that a substantial amount of precursor for lipid biosynthesis is known to be obtained from the degradation of proteins under N-starvation (Sun et al., 2018a), and a recent study demonstrated that normal autophagy activity is essential for the recycling of ribosomal proteins which in turn supports lipid accumulation in *C. reinhardtii* under nitrogen starvation (Couso et al., 2018). Therefore, it is likely that a reduction in the autophagic activity of knockdown mutants contributed to unsubstantial increment in algal lipid by limiting the amount of available precursors for lipid synthesis.

While the ATG8 protein has been widely used as an autophagy indicator in many organisms, western blotting was further used to check

Table 2
Maximum specific growth rate and biomass productivity of *C. reinhardtii* wild-type and mutants.

Strain	Maximum specific growth rate (μ_{max}, d^{-1})	Exponential phase		Stationary phase		Biomass productivity (g/L/d)
		Cell no. × 10^7 (cells/ml)	DCW (g/L)	Cell no. × 10^7 (cells/ml)	DCW (g/L)	
WT	2.194	2.32 ± 0.22	1.70 ± 0.14	2.54 ± 0.15	1.85 ± 0.14	0.453
K1	1.861	1.31 ± 0.15	0.93 ± 0.25	2.13 ± 0.08	1.50 ± 0.07	0.363
K2	1.807	1.22 ± 0.06	0.83 ± 0.11	2.01 ± 0.39	1.48 ± 0.11	0.361
A1	1.908	1.71 ± 0.36	1.23 ± 0.16	2.38 ± 0.27	1.73 ± 0.18	0.423
A2	1.815	1.61 ± 0.30	1.13 ± 0.12	2.20 ± 0.19	1.60 ± 0.04	0.390

Table 3
Pigments composition of *C. reinhardtii* wild-type and mutants.

Pigment (mg/g DCW)	N-repletion					N-starvation				
	WT	K1	K2	A1	A2	WT	K1	K2	A1	A2
Neoxanthin	3.96 ± 0.46	3.90 ± 0.03	3.67 ± 0.43	2.74 ± 0.23	3.66 ± 0.41	0.75 ± 0.05	1.01 ± 0.13	0.89 ± 0.44	0.81 ± 0.29	1.63 ± 0.25
Violaxanthin	1.54 ± 0.70	1.48 ± 0.05	1.37 ± 0.28	1.35 ± 0.26	1.37 ± 0.11	0.79 ± 0.05	0.98 ± 0.05	0.81 ± 0.05	0.81 ± 0.11	1.03 ± 0.08
Lutein	4.19 ± 0.32	3.89 ± 0.32	3.41 ± 0.13	3.36 ± 0.15	3.58 ± 0.33	2.83 ± 0.20	3.46 ± 0.44	2.73 ± 0.03	3.63 ± 0.09	3.47 ± 0.08
Chlorophyll *b*	19.45 ± 2.69	18.90 ± 0.90	18.01 ± 2.09	13.94 ± 1.24	17.65 ± 0.46	5.01 ± 0.43	6.19 ± 0.36	5.52 ± 1.01	5.48 ± 1.14	8.45 ± 0.52
Chlorophyll *a*	19.24 ± 2.35	19.05 ± 1.18	18.10 ± 1.66	15.61 ± 2.19	18.01 ± 0.53	5.19 ± 0.49	6.38 ± 0.26	5.41 ± 0.52	5.78 ± 0.90	8.21 ± 0.53
β-carotene	16.21 ± 1.43	11.70 ± 0.91	14.83 ± 1.03	15.01 ± 1.83	15.06 ± 2.33	10.14 ± 2.26	16.00 ± 0.21	15.69 ± 0.51	23.75 ± 2.53	19.52 ± 2.82
Total carotenoids	25.90 ± 2.91	20.96 ± 1.32	23.29 ± 1.88	22.46 ± 2.46	23.66 ± 2.36	14.51 ± 2.46	21.44 ± 0.05	20.11 ± 0.02	28.99 ± 3.01	25.65 ± 2.57
Unidentified [a] (%)	0.46 ± 0.19	0.16 ± 0.22	0.24 ± 0.34	0.30 ± 0.43	0.18 ± 0.25	0.41 ± 0.59	0.41 ± 0.58	0.50 ± 0.03	0.73 ± 0.36	0.51 ± 0.72

Data are presented as the mean ± standard deviation (SD) of triplicates.
[a] Values are given as the percent contribution of unidentified peaks to total peak area.

the expression pattern of ATG8 protein in wild-type and mutants and thereby confirm whether the observed differences in carotenoids and lipid contents were correlated with autophagy activity (Klionsky et al., 2016). Under optimal growth condition, wild-type showed a low, yet detectable level of ATG8, whereas the ATG8 protein bands were below detection levels in A1 and A2 mutants (Fig. 3). It is worth noting that in K1 and K2 mutants, a faint band of ATG8 could be observed, and this faint band became more apparent upon a longer exposure time (E-supplementary data of this work can be found in the online version of this paper). This suggests that *ATG1* knockdown did not suppress the expression of the downstream *ATG8* gene under growth condition. The results further suggested that the amount of ATG8 sharply increased upon starvation in the wild-type (i.e., ca. 4 times higher than that in N-repletion), indicating an increased autophagy activity (Fig. 3c). The relative band intensities of ATG8/α-Tubulin in K1, K2, A1 and A2 mutants were 0.71 ± 0.16, 0.67 ± 0.15, 0.36 ± 0.21 and 0.33 ± 0.08 arbitrary unit (A.U.), respectively, which significantly lower than that of wild-type (Fig. 3c). Taken together, these data suggest a causal relationship between autophagy activity and the changes in carotenoids and lipid accumulation in *C. reinhardtii*.

It has been observed that nitrogen starvation caused remarkable changes in pigment content and composition in *C. reinhardtii* (Sun et al., 2018a). Importantly, the study showed that higher ROS level under nitrogen starvation is advantageous for the conversion from chlorophyll to carotenoids, whereas co-treatment with an antioxidant decreased the percentage of total carotenoids. Taken together, a model is proposed for the interaction between autophagy and carotenoids in microalgae. In this model, autophagy and carotenoids may act on the opposite sides of the metabolic seesaw in maintaining cellular ROS level: the down-regulation of one side would lead to an enhancement of the other side to compensate the loss in cellular protection capacitance. In this study, a decrease in autophagy activity has been shown to trigger the over-production of β-carotene, a strong antioxidant which could improve stress tolerance of knockdown mutants under nitrogen starvation. A trade-off between carotenoids and lipid biosynthesis is therefore expected, as the two pathways share the same acetyl-CoA precursor (Ma et al., 2019). However, the ability to produce high yield of natural β-carotene, for which a rising demand is expected in coming years, without a substantial compromise in biomass productivity could make this strategy economically viable (Ambati et al., 2019).

3.5. Analysis of fatty acids composition and biodiesel properties

The fatty acids composition of the extracted total lipid was analyzed by gas chromatography (Table 4). After transesterification, fatty acid methyl esters (FAME) in the samples were identified based on a 37-mix FAME standard (Sigma-Aldrich, USA) and quantitated against a heptadecanoic acid internal standard. In all strains, the fatty acids profiles were dominated by C16 and C18 components. Interestingly, knockdown of autophagy led to an increase in saturated fatty acids (SFA) and monounsaturated fatty acids (MUFA) while reduced the polyunsaturated fatty acids (PUFA) portion under both optimal and nitrogen starvation conditions (Fig. 3b and Table 4). As a consequence of nitrogen depletion, the ratio of SFA to UFA was increased from 0.64 to 0.75 in wild-type, whereas it was incremented from 0.69 to 0.83, 0.69 to 0.73, 0.80 to 0.81, and 0.67 to 0.82 in mutant K1, K2, A1, and A2, respectively (Table 4). The biodiesel quality, as measured by cetane number, iodine value, and oxidation stability, was improved under nitrogen starvation in all strains, which agrees well with a previous study, and this improvement was especially pronounced in the mutants due to their higher SFA/UFA ratios (Sun et al., 2018a).

It has been reported that under stress conditions, excess ROS can easily react with PUFA due to the presence of double bonds in their chemical structures, causing the oxidative degradation of lipids called lipid peroxidation (Mylonas and Kouretas, 1999). Once the PUFA is attacked by ROS, it could initiate a chain reaction which eventually

Table 4
Fatty acids composition of *C. reinhardtii* wild-type and mutants.

Fatty acid (weight %)	N-repletion					N-starvation				
	WT	K1	K2	A1	A2	WT	K1	K2	A1	A2
C14:0	2.06 ± 0.86	1.38 ± 0.47	1.47 ± 0.10	2.24 ± 1.01	0.75 ± 0.02	1.90 ± 0.51	2.71 ± 0.35	1.79 ± 0.02	1.39 ± 0.87	0.95 ± 0.14
C16:0	28.81 ± 1.78	32.69 ± 4.21	32.58 ± 2.74	32.75 ± 1.16	33.89 ± 2.78	33.06 ± 2.35	34.14 ± 1.46	34.75 ± 0.27	36.69 ± 0.95	36.34 ± 0.13
C16:1	8.10 ± 0.20	6.48 ± 2.75	8.22 ± 2.24	7.81 ± 0.09	7.11 ± 0.65	7.42 ± 0.32	7.27 ± 1.59	6.62 ± 0.23	7.14 ± 0.44	6.77 ± 0.15
C16:2	1.14 ± 0.17	1.47 ± 0.68	1.19 ± 0.22	1.06 ± 0.01	1.44 ± 0.68	1.10 ± 0.07	1.26 ± 0.16	1.51 ± 0.15	1.19 ± 0.08	1.40 ± 0.47
C16:3	0.72 ± 0.01	1.53 ± 1.04	1.40 ± 1.12	0.68 ± 0.00	1.71 ± 0.37	1.65 ± 1.19	1.21 ± 0.93	2.51 ± 0.04	1.29 ± 0.38	1.32 ± 0.22
C16:4	9.56 ± 1.20	6.00 ± 4.18	5.92 ± 3.17	7.76 ± 0.57	4.35 ± 0.12	6.62 ± 2.48	5.37 ± 1.32	3.56 ± 0.60	3.65 ± 0.03	4.07 ± 0.07
C18:0	8.23 ± 0.64	6.88 ± 3.26	6.68 ± 3.39	9.49 ± 0.29	5.54 ± 0.32	7.99 ± 2.30	8.44 ± 1.02	5.76 ± 0.74	6.64 ± 0.91	7.66 ± 1.83
C18:1	12.98 ± 0.42	18.03 ± 4.06	17.52 ± 4.19	13.85 ± 0.20	19.50 ± 1.36	14.23 ± 0.84	18.69 ± 1.29	20.47 ± 0.84	20.32 ± 0.14	19.27 ± 2.55
C18:2	4.77 ± 0.45	10.38 ± 7.90	8.17 ± 6.85	4.14 ± 0.81	13.07 ± 2.92	7.04 ± 2.97	5.82 ± 2.11	11.43 ± 0.97	9.87 ± 0.17	10.44 ± 0.64
C18:3	23.63 ± 1.58	15.14 ± 7.24	16.86 ± 6.22	20.21 ± 0.37	12.64 ± 1.67	19.00 ± 3.47	15.09 ± 1.68	11.60 ± 0.97	11.81 ± 0.36	11.78 ± 0.35
Total	100.00	100.00	100.00	100.00	100.00	100.00	100.00	100.00	100.00	100.00
SFA	39.10 ± 1.55	40.96 ± 0.48	40.73 ± 0.75	44.48 ± 0.43	40.18 ± 3.12	42.95 ± 0.56	45.29 ± 0.10	42.30 ± 1.03	44.73 ± 0.83	44.95 ± 2.10
MUFA	21.08 ± 0.62	24.51 ± 1.31	25.73 ± 1.95	21.66 ± 0.28	26.61 ± 0.71	21.64 ± 1.16	25.95 ± 0.30	27.09 ± 0.61	27.46 ± 0.30	26.04 ± 2.70
PUFA	39.82 ± 2.17	34.53 ± 1.79	33.54 ± 1.20	33.86 ± 0.15	33.21 ± 2.42	35.41 ± 1.72	28.76 ± 0.20	30.61 ± 0.42	27.82 ± 0.53	29.01 ± 0.60
SFA/UFA	0.64	0.69	0.69	0.80	0.67	0.75	0.83	0.73	0.81	0.82
Biodiesel properties[a]										
CN (≥51)	45.43	49.95	49.78	49.04	51.29	49.01	52.14	52.49	53.70	53.34
IV (≤120)	125.21	105.51	106.11	109.07	99.75	109.32	95.43	94.16	88.82	90.51
Oxidation stability (≥6h)	6.75	7.21	7.31	7.43	7.18	7.12	8.23	7.71	8.03	7.90

[a] Selected specifications from Biodiesel EN 14214 standards. Data are mean ± standard deviation (SD) of triplicates. TFA = total fatty acids; SFA = saturated fatty acids; MUFA = monounsaturated fatty acids; PUFA = polyunsaturated fatty acids; UFA = unsaturated fatty acids; CN = cetane number; IV = iodine value.

results in cellular disruption (Mylonas and Kouretas, 1999). Although additional studies are required, our results suggest that cells with low autophagy activity may redirect their metabolic flux from the biosynthesis of PUFA to SFA and MUFA, while enhancing the production of antioxidant carotenoids such as β-carotene. These actions seem to collectively contribute to overcoming the impaired autophagic functions, thereby promoting cellular survival under nitrogen starvation.

4. Conclusions

The present study has demonstrated that increased carotenoid production can be achieved by regulating autophagic activity via artificial miRNAs-mediated gene silencing. Using this approach, *ATG1* and *ATG8* genes were successfully knockdown in *C. reinhardtii*. The reduction in autophagic activity resulted in the overproduction of β-carotene in all tested mutants under nitrogen starvation. Moreover, the mutants exhibited a metabolic shift towards SFA and MUFA, which in turn seemingly improved the quality of fatty acids as precursors for biodiesel production. This study offers a proof-of-concept that the production of valuable metabolites is enhanced by regulating the seesaw cross-talk between two paired pathways in microalgae.

Acknowledgements

This work was supported by a grant from Marine Biotechnology Program (20150184) funded by Ministry of Oceans and Fisheries, Korea; by the Advanced Biomass R&D Center (ABC) of Global Frontier Project funded by the Ministry of Science and ICT (ABC-2015M3A6A2065697); and by grant from the Korea Research Institute of Bioscience and Biotechnology (KRIBB) Research Initiative Program (www.kribb.re.kr).

Appendix A. Supplementary data

Supplementary data to this article can be found online at https://doi.org/10.1016/j.biortech.2019.121937.

References

Abeliovich, H., Klionsky, D.J., 2001. Autophagy in yeast: mechanistic insights and physiological function. Microbiol. Mol. Biol. Rev. 65 (3), 463–479.
Ahmad, P., Sarwat, M., Sharma, S., 2008. Reactive oxygen species, antioxidants and signaling in plants. J. Plant Biol. 51 (3), 167–173.
Ambati, R.R., Gogisetty, D., Aswathanarayana, R.G., Ravi, S., Bikkina, P.N., Bo, L., Yuepeng, S., 2019. Industrial potential of carotenoid pigments from microalgae: current trends and future prospects. Crit. Rev. Food Sci. Nutr. 59 (12), 1880–1902.
Blaby, I.K., Glaesener, A.G., Mettler, T., Fitz-Gibbon, S.T., Gallaher, S.D., Liu, B., Boyle, N.R., Kropat, J., Stitt, M., Johnson, S., Benning, C., Pellegrini, M., Casero, D., Merchant, S.S., 2013. Systems-level analysis of nitrogen starvation-induced modifications of carbon metabolism in a *Chlamydomonas reinhardtii* starchless mutant. Plant Cell 25 (11), 4305–4323.
Bligh, E.G., Dyer, W.J., 1959. A rapid method of total lipid extraction and purification. Can. J. Biochem. Physiol. 37 (8), 911–917.
Borowitzka, M.A., 2013. High-value products from microalgae—their development and commercialisation. J. Appl. Phycol. 25 (3), 743–756.
Couso, I., Pérez-Pérez, M.E., Martínez-Force, E., Kim, H.-S., He, Y., Umen, J.G., Crespo, J.L., 2018. Autophagic flux is required for the synthesis of triacylglycerols and ribosomal protein turnover in *Chlamydomonas*. J. Exp. Bot. 69 (6), 1355–1367.
Fiedor, J., Burda, K., 2014. Potential role of carotenoids as antioxidants in human health and disease. Nutrients 6 (2), 466–488.
Filomeni, G., De Zio, D., Cecconi, F., 2015. Oxidative stress and autophagy: the clash between damage and metabolic needs. Cell Death Differ. 22 (3), 377–388.
Gimpel, J.A., Henríquez, V., Mayfield, S.P., 2015. In metabolic engineering of eukaryotic microalgae: potential and challenges come with great diversity. Front. Microbiol. 6 (1376), 1–14.
Giordano, S., Darley-Usmar, V., Zhang, J., 2013. Autophagy as an essential cellular antioxidant pathway in neurodegenerative disease. Redox Biol. 2 (2014), 82–90.
Gong, M., Bassi, A., 2016. Carotenoids from microalgae: a review of recent developments. Biotechnol. Adv. 34 (8), 1396–1412.
Heo, J., Shin, D.-S., Cho, K., Cho, D.-H., Lee, Y.J., Kim, H.-S., 2018. Indigenous microalga *Parachlorella* sp. JD-076 as a potential source for lutein production: optimization of lutein productivity via regulation of light intensity and carbon source. Algal Res. 33 (2018), 1–7.
Islam, M., Magnusson, M., Brown, R., Ayoko, G., Nabi, M., Heimann, K., 2013. Microalgal species selection for biodiesel production based on fuel properties derived from fatty acid profiles. Energies 6 (11), 5676–5702.
Klionsky, D.J., Abdelmohsen, K., Abe, A., Abedin, M.J., Abeliovich, H., Acevedo Arozena, A., Adachi, H., Adams, C.M., Adams, P.D., Adeli, K., et al., 2016. Guidelines for the use and interpretation of assays for monitoring autophagy. Autophagy 12 (1), 1–222.
Lee, J.-Y., Yoo, C., Jun, S.-Y., Ahn, C.-Y., Oh, H.-M., 2010. Comparison of several methods for effective lipid extraction from microalgae. Bioresour. Technol. 101 (1), S75–S77.
Liu, W., Huang, Z., Li, P., Xia, J., Chen, B., 2012. Formation of triacylglycerol in *Nitzschia closterium f. minutissima* under nitrogen limitation and possible physiological and biochemical mechanisms. J. Exp. Mar. Biol. Ecol. 418-419 (2012), 24–29.
Liu, Y., Bassham, D.C., 2012. Autophagy: pathways for self-eating in plant cells. Annu. Rev. Plant Biol. 63 (1), 215–237.
Lohr, M., 2009. Chapter 21 – carotenoids. In: Harris, E.H., Stern, D.B., Witman, G.B. (Eds.), The Chlamydomonas Sourcebook (Second Edition). Academic Press, London, pp. 799–817.
López García de Lomana, A., Schäuble, S., Valenzuela, J., Imam, S., Carter, W., Bilgin, D.D., Yohn, C.B., Turkarslan, S., Reiss, D.J., Orellana, M.V., Price, N.D., Baliga, N.S., 2015. Transcriptional program for nitrogen starvation-induced lipid accumulation in *Chlamydomonas reinhardtii*. Biotechnol. Biofuels 8 (2015), 1–18.
Ma, T., Shi, B., Ye, Z., Li, X., Liu, M., Chen, Y., Xia, J., Nielsen, J., Deng, Z., Liu, T., 2019. Lipid engineering combined with systematic metabolic engineering of *Saccharomyces cerevisiae* for high-yield production of lycopene. Metab. Eng. 52 (2019), 134–142.
Mallick, N., Mohn, F.H., 2000. Reactive oxygen species: response of algal cells. J. Plant Physiol. 157 (2), 183–193.
Mata-Gómez, L.C., Montañez, J.C., Méndez-Zavala, A., Aguilar, C.N., 2014. Biotechnological production of carotenoids by yeasts: an overview. Microb. Cell Fact. 13 (2014), 12–23.
Menon, K.R., Balan, R., Suraishkumar, G.K., 2013. Stress induced lipid production in *Chlorella vulgaris*: relationship with specific intracellular reactive species levels. Biotechnol. Bioeng. 110 (6), 1627–1636.
Minhas, A.K., Hodgson, P., Barrow, C.J., Adholeya, A., 2016. A review on the assessment of stress conditions for simultaneous production of microalgal lipids and carotenoids. Front. Microbiol. 7 (2016), 546–560.
Molnar, A., Bassett, A., Thuenemann, E., Schwach, F., Karkare, S., Ossowski, S., Weigel, D., Baulcombe, D., 2009. Highly specific gene silencing by artificial microRNAs in the unicellular alga *Chlamydomonas reinhardtii*. Plant J. 58 (1), 165–174.
Mylonas, C., Kouretas, D., 1999. Lipid peroxidation and tissue damage. Vivo 13 (3), 295–309.
Nakatogawa, H., Ichimura, Y., Ohsumi, Y., 2007. Atg8, a ubiquitin-like protein required for autophagosome formation, mediates membrane tethering and hemifusion. Cell 130 (1), 165–178.
Nimse, S.B., Pal, D., 2015. Free radicals, natural antioxidants, and their reaction mechanisms. RSC Adv. 5 (35), 27986–28006.
Ossowski, S., Schwab, R., Weigel, D., 2008. Gene silencing in plants using artificial microRNAs and other small RNAs. Plant J. 53 (4), 674–690.
Pérez-Pérez, M.E., Couso, I., Crespo, J.L., 2012. Carotenoid deficiency triggers autophagy in the model green alga *Chlamydomonas reinhardtii*. Autophagy 8 (3), 376–388.
Pérez-Pérez, M.E., Couso, I., Heredia-Martínez, L.G., Crespo, J.L., 2017. Monitoring autophagy in the model green microalga *Chlamydomonas reinhardtii*. Cells 6 (4), 36–46.
Ramanan, R., Tran, Q.-G., Cho, D.-H., Jung, J.-E., Kim, B.-H., Shin, S.-Y., Choi, S.-H., Liu, K.-H., Kim, D.-S., Lee, S.-J., Crespo, J.L., Lee, H.-G., Oh, H.-M., Kim, H.-S., 2018. The ancient phosphatidylinositol 3-kinase signaling system is a master regulator of energy and carbon metabolism in algae. Plant Physiol. 177 (3), 1050–1065.
Sathasivam, R., Ki, J.-S., 2018. A review of the biological activities of microalgal carotenoids and their potential use in healthcare and cosmetic industries. Mar. Drugs 16 (1), 26–37.
Schieber, M., Chandel, N.S., 2014. ROS function in redox signaling and oxidative stress. Curr. Biol. 24 (10), R453–R462.
Shi, K., Gao, Z., Shi, T.-Q., Song, P., Ren, L.-J., Huang, H., Ji, X.-J., 2017. Reactive oxygen species-mediated cellular stress response and lipid accumulation in oleaginous microorganisms: the state of the art and future perspectives. Front. Microbiol. 8 (2017), 793–801.
Sui, Y., Muys, M., Van de Waal, D.B., D'Adamo, S., Vermeir, P., Fernandes, T.V., Vlaeminck, S.E., 2019. Enhancement of co-production of nutritional protein and carotenoids in *Dunaliella salina* using a two-phase cultivation assisted by nitrogen level and light intensity. Bioresour. Technol. 287 (2019), 121398–121406.
Sun, H., Mao, X., Wu, T., Ren, Y., Chen, F., Liu, B., 2018a. Novel insight of carotenoid and lipid biosynthesis and their roles in storage carbon metabolism in *Chlamydomonas reinhardtii*. Bioresour. Technol. 263 (2018), 450–457.
Sun, X.-M., Ren, L.-J., Zhao, Q.-Y., Ji, X.-J., Huang, H., 2018b. Microalgae for the production of lipid and carotenoids: a review with focus on stress regulation and adaptation. Biotechnol. Biofuels 11 (1), 272–287.
Takaya, T., Anan, M., Iwata, K., 2018. Vibrational relaxation dynamics of β-carotene and its derivatives with substituents on terminal rings in electronically excited states as studied by femtosecond time-resolved stimulated Raman spectroscopy in the near-IR region. PCCP 20 (5), 3320–3327.
Tran, Q.-G., Cho, K., Park, S.-B., Kim, U., Lee, Y.J., Kim, H.-S., 2019. Impairment of starch biosynthesis results in elevated oxidative stress and autophagy activity in *Chlamydomonas reinhardtii*. Sci. Rep. 9 (1), 9856–9864.
Valledor, L., Furuhashi, T., Recuenco-Muñoz, L., Wienkoop, S., Weckwerth, W., 2014. System-level network analysis of nitrogen starvation and recovery in *Chlamydomonas reinhardtii* reveals potential new targets for increased lipid accumulation. Biotechnol. Biofuels 7 (1), 171–187.
Wong, P.-M., Puente, C., Ganley, I.G., Jiang, X., 2013. The ULK1 complex: sensing nutrient signals for autophagy activation. Autophagy 9 (2), 124–137.
Yilancioglu, K., Cokol, M., Pastirmaci, I., Erman, B., Cetiner, S., 2014. Oxidative stress is a

mediator for increased lipid accumulation in a newly isolated *Dunaliella salina* strain. PLoS ONE 9 (3), e91957–e91969.
Yun, J.-H., Cho, D.-H., Heo, J., Lee, Y.J., Lee, B., Chang, Y.K., Kim, H.-S., 2019. Evaluation of the potential of *Chlorella* sp. HS2, an algal isolate from a tidal rock pool, as an industrial algal crop under a wide range of abiotic conditions. J. Appl. Phycol. 1–14.
Zhang, Z., Sun, D., Cheng, K.-W., Chen, F., 2018. Inhibition of autophagy modulates astaxanthin and total fatty acid biosynthesis in *Chlorella zofingiensis* under nitrogen starvation. Bioresour. Technol. 247 (2018), 610–615.
Zhao, Y., Wang, H.-P., Han, B., Yu, X., 2019. Coupling of abiotic stresses and phytohormones for the production of lipids and high-value by-products by microalgae: a review. Bioresour. Technol. 274 (2019), 549–556.